



HAL
open science

Improved corrosive wear resistance of carbidic austempered ductile iron by addition of Cu

Penghui Yang, Hanguang Fu, Rafik Absi, Rachid Bennacer, Jian Lin, Xingye Guo

► **To cite this version:**

Penghui Yang, Hanguang Fu, Rafik Absi, Rachid Bennacer, Jian Lin, et al.. Improved corrosive wear resistance of carbidic austempered ductile iron by addition of Cu. *Materials Characterization*, 2020, 168, pp.110577 -. 10.1016/j.matchar.2020.110577 . hal-03492523

HAL Id: hal-03492523

<https://hal.science/hal-03492523v1>

Submitted on 5 Sep 2022

HAL is a multi-disciplinary open access archive for the deposit and dissemination of scientific research documents, whether they are published or not. The documents may come from teaching and research institutions in France or abroad, or from public or private research centers.

L'archive ouverte pluridisciplinaire **HAL**, est destinée au dépôt et à la diffusion de documents scientifiques de niveau recherche, publiés ou non, émanant des établissements d'enseignement et de recherche français ou étrangers, des laboratoires publics ou privés.



Distributed under a Creative Commons Attribution - NonCommercial 4.0 International License

Improved Corrosive Wear Resistance of Carbide Austempered Ductile Iron by Addition of Cu

Penghui Yang^{1,2}, Hanguang Fu^{1*}, Rafik Absi^{3*}, Rachid Bennacer³, Jian Lin¹, Xingye Guo¹

(1. Key Laboratory of Advanced Functional Materials, Ministry of Education, School of Materials Science and Engineering, Beijing University of Technology, Beijing 100124, P. R. China; 2. CY Cergy Paris University, 33 Boulevard du Port, 95011 Cergy Pontoise Cedex, France; 3. ECAM-EPMI Graduate School of Engineering, 13 Boulevard de l'Hautil, 95092, Cergy-Pontoise Cedex, France)

1* Correspondence address:

Corresponding author: Prof. Fu Hanguang

Address: School of Materials Science and Engineering,

Beijing University of Technology,

Number 100, Pingle Garden,

Chaoyang District,

Beijing 100124,

P. R. China

E-mail: hgfu@bjut.edu.cn

Fax: +86-10-67396244

Tel: +86-10-67396093

2* Correspondence address:

Corresponding author: Prof. Rafik Absi

Address: ECAM-EPMI

13, Bd de l'Hautil - 95092 Cergy-Pontoise Cedex

E-mail: r.absi@ecam-epmi.com

Tel: 01 30 75 69 32

Abstract

In this work, **different contents of Cu were added** into carbidic austempered ductile iron (CADI) to improve the corrosion resistance and the corrosive wear resistance. Microstructures of CADI have been systematically investigated by scanning electron microscope (SEM), transmission electron microscopy (TEM), X-ray diffraction (XRD), atomic force microscope (AFM). The results showed that with the addition of Cu elements, the thickness of bainitic ferrite plates and the potential difference ($\Delta U_{\text{matrix-graphite nodules}}$ and $\Delta U_{\text{matrix-carbides}}$) were reduced significantly. The effect of Cu on the corrosion resistance and the corrosive wear resistance has been studied by an electrochemical workstation and two kinds of corrosive wear tester. **In addition, worn surfaces and corroded surfaces of the samples have been examined** by SEM, 3D laser scanning microscope and X-ray photoelectron spectroscopy (XPS). **As the Cu content increased, the corrosion resistance of CADI under acidic condition increased.** When the Cu content **was** 1 wt.%, both corrosive wear resistance without load under alkaline condition and corrosive wear resistance with load under **alkaline and acidic** condition were optimal. Nevertheless, under acidic condition, the corrosive wear resistance without load of CADI with 1.5 wt% Cu was optimal.

Key words : Carbidic Austempered Ductile Iron; Cu element; Corrosion resistance; Wear resistance; TEM; AFM

Highlights

- (1) Electrochemical potentials of CADI's microstructural components is: $U_{\text{graphite}} > U_{\text{carbides}} > U_{\text{matrix}}$.
- (2) Cu element is mainly distributed in the retained austenite.
- (3) The corrosion resistance of CADI can be improved by adding Cu element
- (4) Corrosive wear resistance of CADI with 1 wt.% Cu is significantly better than that of Cu-free CADI.

1. Introduction

It is of widespread knowledge that corrosion and wear are important mechanisms of degradation of materials that cause failure. Compared with the dry wear conditions, wear under corrosive conditions can either lead to a fast degradation or failure [1-5]. The wear behavior of metallic materials under corrosive conditions strongly depends on the characteristics (composition, thickness, et al) of the corrosive layer which is formed at the interface of the contacting materials [6], as well as the selected wear conditions [7] and corrosion solution [8]. Thus the study on the corrosive layer formed in different corrosive solutions and the surface layer formed under different wear conditions are very important for revealing the corrosion and wear behavior of metallic materials [9-10].

The properties (e.g. hardness, impact toughness, tensile strength, and wear resistance) of carbidic austempered ductile iron (CADI) have been significantly improved after several works regarding processing design and composition control [11-15]. CADI is widely applied in the engineering field [16]. After Ti refinement, the maximum diameter of graphite nodules decreased from 58 to 40 μm , and the shape of carbides transformed from linked network to dispersed. The hardness of Ti-bearing CADI was 3.5 HRC higher than ordinary CADI, and the impact toughness was increased by 14.3%. Besides, due to the decrease in exfoliation, the weight loss of Ti-bearing CADI was 14.8% lower than ordinary CADI [12]. With the addition of 0.06 wt.% nano-cerium oxide into CADI containing 3.5C-2.85Si-0.75Cr wt.%, the impact toughness was improved by 33%, and the abrasive wear rate was reduced 29%

[13]. A CADI composed by a superfine ausferrite matrix and many particles could be obtained by S&A treatment. This CADI had an impact toughness 120% higher than the traditional CADI without sacrificing hardness, and had excellent wear resistance under high wear load [14]. **However, research on improving corrosion and corrosive wear resistance of CADI has not been reported.**

Cu element is often added into steel and iron to increase the corrosion resistance and the corrosive wear resistance [17-19]. Tomio et al. [17] studied the role of alloyed copper on the corrosion resistance of austenitic stainless steel in H_2S-Cl^- environment, and found that the alloyed Cu improved the stress corrosion cracking (SCC) resistance of austenitic stainless steels. In addition, the alloyed Cu prevented the decrease in the pitting corrosion resistance. Hong et al. [18] researched the corrosion behavior of copper containing low alloy steels in sulphuric acid, and found that the corrosion resistance of low alloy steel in sulphuric acid was significantly improved by adding 0.2-0.35 wt.% copper. Additionally, the improvement of corrosion resistance was attributed to the high hydrogen overpotential suppressing the cathodic hydrogen evolution reaction. **Zhou et al. [19] found the corrosion and the wear resistance of ductile iron was significantly improved after adding Cu element. When the Cu content increased from 0 wt.% to 0.5 wt.%, the wear resistance increased by 20.9 % and the corrosion potential rose by 0.13 V. However, there are a few reports about improving the corrosive wear resistance of CADI by adding Cu element at present.**

In this study, **different contents of Cu are** added into carbidic austempered ductile iron. The objective is to improve the corrosive wear resistance of CADI, and to

investigate how the Cu element affects microstructure, corrosion resistance and corrosive wear resistance. The results will provide theoretical guidance and experimental support for the application of CADI in a variety of complex environments.

2. Experiment details

2.1. Material preparation

All raw materials were processed using a 50 kg medium frequency induction furnace. The electrolytic copper was added into molten iron at 1450 °C, added 0.15 wt.% pure aluminum to deoxidize after heating to 1520 °C, transferred into the ladle before added 1.2 wt.% inoculant (75 wt.% Si) and 1.5 wt.% nodularizer (6Mg-2Re-40 wt.% Si); finally poured into the sand molds at 1400 °C, obtaining Y-block ingots following ASTM A781/A 781-M95. In order to study the effect of Cu on CADI, 0, 0.5, 1.0, 1.5, 2.0 wt.% Cu were introduced into the carbidic ductile iron with a basic composition of 3.72C-2.77Si-0.51Mn-0.99Cr (wt.%), respectively. Samples were cut from the bottom of the Y-block ingots for heat treatment. The heat treatment process is as follows: samples were austenitized at 900 °C for 120 min, and then quenched into a salt bath (50 wt.% KNO₃ + 50 wt.% NaNO₃) held at 300 °C for 120 min before final cooling to room temperature.

2.2. Microstructural examination

The volume fraction of austenite, the volume fraction of ferrite and the carbon content of austenite were estimated by Rigaku-Utima-IV X-ray diffractometer (XRD).

The detailed estimation steps and methods could be found in published results [5]. **Cu-K α radiation was used at 30 kV and 40 mA.** XRD specimens were scanned in the angular 2θ range from 20° to 100° with a step size of $0.5^\circ/\text{min}$ and a collection time of 10 s. **The microstructures of the samples examined with** a JSM-6510 scanning electron microscope (SEM) with an energy dispersive spectrometer (EDS) and a JEM-2100F transmission electron microscopy (TEM) with an energy dispersive X-ray (EDX). **The potential of graphite, carbide and matrix was measured by a Bruker MultiMode atomic force microscope (AFM) with PeakForce KPFM capability [20].** Besides, the elemental composition and valence state of the sample surface were analyzed by an ESCALAB 250 Xi-type X-ray photoelectron spectroscopy (XPS) [21-22], **and worn surface of the samples** was investigated by a VK-9710 3D laser scanning microscope.

2.3 Corrosion resistance tests

The corrosion resistance tests were carried out by a CHI600A electrochemical workstation at room temperature. **A cell composed of three electrodes was used, including a platinum sheet as a counter electrode; a saturated calomel electrode (SCE) as a reference electrode; and the samples as the working electrode (WE), for the electrochemical impedance spectroscopy (EIS) measurements.** The WE area was **fixed at 1 cm^2 , and the samples were ground and polished before the tests.** All samples were rinsed in deionized water followed by immersion in the sulfuric acid solution of $\text{pH} = 4$ for 30 min to stabilize the open circuit potential value. EIS tests were performed over a frequency ranging from 100 kHz to 0.1 Hz.

2.4 Corrosive wear tests

Prismatic specimens with a size of $6 \times 16 \times 52$ mm were cut by electrical discharge machining and surface oxide layers were removed after heat treatment. Corrosive wear samples with a size of $5 \times 15 \times 50$ mm were polished by a mechanical method. The erosive wear tests were carried out in a ML-10 erosion tester with a speed of 200 r/min and a test time of 10 h, and the working principle has been presented in published papers [5]. The slurry was prepared with water and 200-300 μm quartz sand according to a volume ratio of 1:1, and the pH of slurry was adjusted by sulfuric acid and sodium hydroxide. In this work, the weight loss of CADI for each Cu content was respectively measured in the different slurry with pH = 4 and pH = 10, and the average value of three samples was calculated as the final result.

To further compare the difference of corrosive wear with load and without load, the weight loss of CADI was tested by the MLS-225 wet rubber wheel wear tester, and the working principle was shown in Fig. 1. The rubber wheel was in direct contact with the sample with a size of $6 \times 25 \times 60$ mm, and rotated in counterclockwise direction. According a volume ratio of 1:1, the aqueous solution with different pH value and the quartz sand with a size of 100-150 μm were mixed to prepare the slurry. In order to distinguish them from the corrosive wear performed by ML-10 erosion tester, the tests were called “corrosive wear with load tests (CWWL tests)” below. The test parameters were as follows: a speed of 200 r/min, a test time of 30 min and a weight of 1 kg (the normal force of the sample is about 40 N). Similarly, for the CWWL tests, the weight loss of CADI for each different Cu content was

respectively measured in the different slurry with pH = 4 and pH = 10. The weight of the samples was measured by a TG328B balance with a minimum resolution of 0.01 mg, and the average value of three samples was taken as the weight loss result.

3. Results and discussion

3.1 Effects of Cu on microstructures of CADI

The microstructures of CADI consisted of graphite nodules, carbides and matrix, and the matrix consisted of bainitic ferrite laths and retained austenite, as shown in Fig. 2. With the increase of Cu content, the retained austenite increased, furthermore the Cu content reached 2 wt.%, the bulk-like retained austenite appeared in the matrix, Fig. 2e. The amount of retained austenite of CADI for different Cu content was calculated by the method from Ref [5,15], and the results showed that the amount of retained austenite gradually increased from 21.3 % to 26.9 % with the rise of Cu content from 0 wt.% to 2 wt.%. After adding Cu, the rate that undercooled austenite transformed into bainite was decreased [15, 23], which led to the increase of retained austenite. The volume fraction of carbides was measured by the analysis of OM images with an Image-pro software. Results showed that with the rise of Cu content from 0 wt.% to 2 wt.%, the quantity of carbides decreased from 13.2 vol.% to 11.5 vol.%.

To study the microstructure evolution and the existing forms of Cu elements, the microstructures of Cu-free CADI and Cu-bearing CADI were compared by transmission electron microscopy (TEM), and the results were shown in Fig. 3. The

thickness of bainitic ferrite in Cu-free CADI was about 100 - 200 nm, while the thickness of bainitic ferrite in CADI with 2.0 wt.% Cu was about 70 - 150 nm, which indicated that the thickness of bainitic ferrite laths reduced after adding 2.0 wt% Cu. Cu could prevented the diffusion of C element in CADI, which inhibited the growth of ferrite. Therefore, with the addition of Cu thickness of bainitic ferrite laths was reduced. Bright-field TEM micrographs and corresponding selected area diffraction patterns (SADPs) results showed that the bainitic ferrite had a body-centered cubic (BCC) structure with a lattice constant of $a = b = c = 0.2866$ nm, without precipitated carbides on its surface, as shown in Fig.3b. Fig. 3c was the result of SADPs from area C in Fig. 3b. The retained austenite had a face-centered cubic (FCC) structure with a lattice constant of $a = b = c = 0.3612$ nm, and the carbide had an orthorhombic lattice with a lattice constant of $a = 0.50153$ nm, $b = 0.68416$ nm, $c = 0.43817$ nm. Additionally, no Cu-rich compounds were found in the Cu-bearing CADI by using TEM and EDX, indicating that Cu-rich compounds might not be formed after adding 2.0 wt.% Cu to the carbidic ductile iron. EDX tested results showed that most Cr elements were distributed in carbides, while most Cu elements were distributed in retained austenite, as shown in Fig. 3d. In other words, Cr elements were enriched in eutectic carbides to form $(Fe, Cr)_3C$ type carbides, while Cu elements were dissolved in retained austenite to form solid solution.

3.2 Effects of Cu on corrosion resistance of CADI

In order to evaluate the corrosion resistance of CADI under acidic conditions, the electrochemical impedance spectroscopy (EIS) of CADI for each different Cu content

was tested by an electrochemical workstation. Nyquist plots of samples exposed to acidic solutions with pH = 4 are shown in Fig. 4. When CADI was in contact with acidic solutions, an immediate attack on the metal took place with the formation of hydrogen gas and ferrous ions, as shown in Eq.(1)

Anodic reaction:



Cathodic reaction:



From Fig. 4, it was revealed that all plots showed a depressed semicircle pattern in the whole frequency range, indicating that only one time constant exists between the interface of the solid electrode and the solution. As the increases of Cu content, the impedance value increased, which indicated that the higher the Cu content, the better the corrosion resistance of CADI. The potential difference between the matrix and other phases might be the main mechanism of CADI's corrosion failure [19]. After adding Cu, the potential difference decreased. Therefore, with the addition of Cu, the corrosion resistance of CADI improved.

3.3 Effects of Cu on Corrosive wear of CADI

To study the effect of Cu on the corrosive wear resistance of CADI, the weight loss of CADI for each different Cu content in the slurry were calculated in this work, and the changes of the weight loss with time were shown in Fig. 5. The weight loss of CADI was almost linear with the time, as shown in Fig. 5a and Fig. 5b, which

indicated that the weight loss per time interval was approximately constant. Under acidic conditions, the weight loss was much higher than alkaline conditions. The corrosive wear resistance of CADI has been significantly improved after adding a small amount of Cu element (0 - 1.0 wt.%). However, with the further rise of Cu content, the retained austenite increased, which led to the decrease of hardness. Therefore, the wear resistance of CADI decreased significantly as the increase of Cu content, especially, above 1.5 wt.%. The optimal corrosive wear resistance of CADI for the acidic and the alkaline conditions was found for 1.5 wt.% Cu and 1.0 wt.% Cu respectively.

The corrosive wear resistance under load of CADI was investigated by CWWL tests, and the relationship between weight loss and Cu content of CADI in acidic and alkaline slurry was shown in Fig. 6. The results showed that the corrosive wear resistance under load of CADI in the acidic slurry was slightly lower than that in the alkaline slurry. With the increase of Cu content, the weight loss decreased firstly and then increased. Noting that the wear resistance of CADI for the both conditions was best when Cu content was 1 wt.%.

3.4 Corrosion behavior of CADI

The potential difference between the phases in CADI was measured by an atomic force microscope (AFM). The results showed that the brightness of the graphite nodules in potential map scanning was significantly higher than the matrix, as shown in Fig. 7a and 7b. The potential difference $\Delta U_{\text{gra-mat}}$ of Cu-free CADI was about 389 - 408 mV (Fig. 7a), and the potential difference $\Delta U_{\text{gra-mat}}$ of CADI with 1.5 wt% Cu was

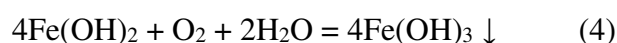
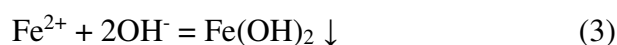
about 305 - 316mV (Fig. 7b), indicating that the potential difference between matrix and graphite nodule was reduced after adding Cu element. Fig. 7c showed the potential distribution of phase around carbides. The potential of carbides was slightly higher than matrix, and the potential difference $\Delta U_{\text{car-mat}}$ between carbides and matrix was about 39 - 47 mV. Therefore, electrochemical potentials of CADI's microstructural components should be: $U_{\text{graphite}} > U_{\text{carbides}} > U_{\text{matrix}}$.

After soaking the CADI with 1.5 wt.% Cu in a sulfuric acid solution with pH = 4 for 3 days, the surface morphology was observed by a scanning electron microscope, as shown in Fig. 8. Large corrosion products with a diameter of 500 μm could be observed on the sample surface, and some cracks and pits were distributed around graphite nodules and carbides. So the corrosion began preferentially from the matrix around graphite nodules and carbides under acidic conditions. EDS results showed that the contents of copper and oxygen around the graphite nodules were slightly higher, which indicated that Cu element in matrix and oxygen element in solution could be bonded to form oxides.

To reveal the corrosion behavior of CADI in solutions with different pH values, the sample was soaked in an alkaline solution with pH = 10 for 3 days and then taken out to obtain the corroded specimen. Surface of corroded specimen was observed by a scanning electron microscope, and some corrosion products were analyzed by EDS. Unlike the acidic conditions, some filiform white corrosion products and a small amount of large corrosion pits occurred on the surface of the sample, as shown in Fig. 9a. It was found that Mg and O elements were enriched in the large corrosion pit.

Therefore, the corrosion products might be the hydroxide which formed by the combination of retained Mg in cast iron and OH⁻ in alkaline solution.

The surface elements and valence of CADI soaked in solution with pH = 10 for 3 days were tested by XPS, and the tested results were presented in Fig. 10 and Fig. 11. There might be a large amount of oxides and hydroxides on the soaked surface, where were Cr₂O₃, Fe₂O₃, Fe₃O₄, Fe(OH)₂, Fe(OH)₃ et al. In addition, the surface of Cu-free CADI soaked in alkaline solution might be following reaction:



After the addition of Cu, the changes of Fe 2p, O 1s and Cr 2p were not significantly different compared with Cu-free CADI. Cu element on the sample surface exists in the form of Cu₂O, as shown in Fig. 11d. This oxide distributed on the surface of CADI could effectively protect the surface of material to reduce the corrosion from corrosive liquid. Therefore, this might be one of the reasons why the corrosion resistance of CADI increased after adding Cu element.

3.5 Wear behavior of CADI

To reveal the corrosive wear failure mechanism of CADI, the corrosive worn surface morphologies of CADI for each different Cu content were investigated by a scanning electron microscope and a 3D laser scanning microscope. The large spherical pits and the small pits with a size of about 1 - 3 μm could be observed on the sample surface after worn in the acidic slurry. In addition, the corrosive worn surface contained a large amount of scratches, as shown in Fig. 12a and 12b. Due to the

increase of corrosion resistance, the amount of small pits in CADI with 1.5 wt% Cu was less than Cu-free CADI. After testing in alkaline slurry, flake shaped graphite, scratches and small pits could be observed on the worn sample surface, Fig. 12c and 12d. The measurements from 3D laser microscope showed that the corrosive wear depth of CADI with 1 wt.% Cu was lower than Cu-free CADI, which might be attributed to the decrease of bainite ferrite in size after adding Cu element.

To further compare the difference between corrosive wear and corrosive wear with load, the worn surface morphologies obtained by CWWL tests were observed by a scanning electron microscope and a 3D laser microscope, Fig. 13. A small amount of graphite and a large number of grooves could be observed on the worn surface after CWWL tests in acidic slurry, as shown in Fig. 13a and 13b. Besides, the roundness and the size of graphite nodules decreased. Under alkaline conditions, the worn surface consisted of many grooves and little graphite. Unlike the corrosive wear surface morphology, no small pits and obvious traces of graphite exuviations were observed on the worn surface after CWWL tests under the two conditions. Therefore, the worn surface obtained by CWWL tests showed the characteristics of abrasive wear. 3D laser morphologies measurements showed that the wear scar depth of CADI with 1 wt% Cu worn in alkaline slurry was the smallest.

4. Conclusions

In this paper, the corrosion resistance and wear resistance of CADI were improved by adding Cu element, and the wear behavior of CADI under different wear

conditions was discussed. The main conclusions are as follows:

(1) With the increase of Cu content from 0 wt.% to 2.0 wt.%, the amount of retained austenite gradually increased from 21.3 % to 26.9 %, and the thickness of bainitic ferrite is reduced from 100 - 200 nm to 70 - 150 nm.

(2) The corrosion resistance of Cu-bearing CADI in acidic solution is significantly better than Cu-free CADI.

(3) When the Cu content is 1 wt.%, the corrosive wear resistance without load under alkaline condition and the corrosive wear resistance with load **under acidic and alkaline condition** are optimal. However, when the Cu content is 1.5 wt.%, the corrosive wear resistance without load under acidic condition is optimal.

(4) Cu elements in CADI are mainly distributed in retained austenite, which can reduce the potential difference between the matrix and graphite nodules and carbides. Besides, under the alkaline solution, Cu_2O can be formed on the sample surface to increase the corrosion resistance of CADI.

Acknowledgement

The authors would like to thank the financial support for this work from National Natural Science Foundation of China under grant (51775006).

References

[1] N. Diomidis, J.P. Celis, P. Ponthiaux, F. Wenger, A methodology for the

assessment of the tribocorrosion of passivating metallic materials, *Lubr. Sci.* 2009; **21**: 53-67.

[2] J. Jiang, M.M. Stack, A. Neville, Modelling the tribo-corrosion interaction in aqueous sliding conditions, *Tribol. Int.* 2002; **35**: 669-679.

[3] R.J.K. Wood, Erosion-corrosion interactions and their effect on marine and offshore materials, *Wear.* 2006; **261**: 1012-1023.

[4] E. Huttunen-Saarivirtaa, E. Isotahdona, J. Metsäjokia, T. Salminenb, L. Carpéna, H. Ronkainen, Tribocorrosion behaviour of aluminium bronze in 3.5wt.% NaCl solution, *Corros. Sci.* 2018; **144**: 207-223

[5] P.H. Yang, H.G. Fu, X.W. Zhao, J. Lin, Y.P. Lei, Wear behavior of CADI obtained at different austenitizing temperatures, *Tribol. Int.* 2019; **140**: 105876

[6] I. Garcia, D. Drees, J.-P. Celis, Corrosion-wear of passivating materials in sliding contacts based on a concept of active wear track area, *Wear.* 2001; **249**: 452-460

[7] A. Iwabuchi, J.W. Lee, M. Uchidate, Synergistic effect of fretting wear and sliding wear of Co-alloy and Ti-alloy in Hanks' solution, *Wear* 2007; **263**: 492-500.

[8] N.K. Tse, N.P. Suh, Chemical effects in sliding wear of aluminum, *Wear.* 1977; **44**: 145-162

[9] S.Z. Wei, L.J. Xu, Review on research progress of steel and iron wear-resistant material, *Acta. Metall. Sinica.*, 2020; **56**: 523-538.

[10] Z. Huang, J. Xing, L. Lv, Effect of tungsten addition on the toughness and hardness of Fe₂B in wear-resistant Fe-B-C cast alloy, *Mater. Charact.* 2013; **75**: 63-68

[11] H.Q. Cheng, H.G. Fu, J. Lin, Y. Lei, Effect of Cr content on microstructure and mechanical properties of carbidic austempered ductile iron, *Mater. Test.* 2018; **60**: 31-39

[12] P.H. Yang, H.G. Fu, R. Nan, X.Y. Guo, J. Lin, Y.P. Lei, Effect of Ti modification on microstructures and properties of carbidic austempered ductile iron, *J. Mater. Eng. Perform.* 2019; **28**: 2335-2347

[13] X. Sun, Y. Wang, D.Y. Li, C. Wang, X. Li, Z.W. Zou, Solid particle erosion behavior of carbidic austempered ductile iron modified by nanoscale ceria particles,

Mater. Des, 2014; **10**: 367-374

[14] P.H. Yang, H.G. Fu, G.L. Li, J.H. Liu, X.B. Zhao, Microstructures and properties of carbidic austempered ductile iron containing Fe₃C particles and superfine ausferrite, Mater. Des. 2020; **186**: 108363

[15] R. Nan, H. Fu, S. Ma, P. Yang, J. Lin, X. Guo, Y. Lei, Microstructure and properties of Cu-bearing carbidic austempered ductile iron, Int J Mater Res. 2019; **110**(7): 621-635

[16] M. Lagarde, A. Basso, J.A. Sikora, R.C. Dommarco, Development and characterization of a new type of ductile iron with a novel multiphase microstructure, ISIJ Int., 2011; **51**: 645-650

[17] A. Tomio, M. Sagara, T. Doi, H. Amaya, N. Otsuka, T. Kudo, Role of alloyed copper on corrosion resistance of austenitic stainless steel in H₂S–Cl-environment, Corros. Sci., 2014; **81**: 144-151

[18] J.H. Hong, S.H. Lee, J.G. Kim, J.B. Yoon, Corrosion behaviour of copper containing low alloy steels in sulphuric acid, Corros. Sci. 2012; **54**: 174-182

[19] Y. Zhou, Z. Lu, M. Zhan, An investigation of the erosion–corrosion characteristics of ductile cast iron, Mater. Des, 2007; **28**: 260-265

[20] M. Mohedano, C. Blawert, K.A. Yasakau, R. Arrabal. E. Matykina, B. Mingo, N. Scharnagl, M.G.S. Ferreira, M.L. Zheludkevich, Characterization and corrosion behavior of binary Mg-Ga alloys, Mater. Charact, 2017; **128**: 85-99

[21] P. Datta, P. Majewski, F. Aldinger, Study of gadolinia-doped ceria solid electrolyte surface by XPS, Mater. Charact, 2009; **60**: 138-143

[22] D. Prusty, A. Pathak, M. Mukherjee, B. Mukherjee, A. Chowdhury, TEM and XPS studies on the faceted nanocrystals of Ce_{0.8}Zr_{0.2}O₂, Mater. Charact, 2015; **100**: 31-35

[23] M. Górny, E. Tyrała, H. Lopez, Effect of copper and nickel on the transformation kinetics of austempered ductile iron, J. Mater. Eng. Perform. 2014; **23**: 3505–3510

List of Figure Captions

Fig. 1 Schematic diagram of corrosive wear with load test (CWWL test)

Fig. 2 SEM images of CADI for different Cu content: (a) 0 wt.% Cu; (b) 0.5 wt.% Cu; (c) 1 wt.% Cu; (d) 1.5 wt.% Cu; (e) 2 wt.% Cu;

Fig. 3 TEM images of Cu-bearing CADI: (a) Bright-field TEM micrographs of Cu-free CADI; (b) Bright-field TEM micrographs of CADI with 2.0 wt.% Cu; (c) Selected area diffraction patterns (SADPs) of area C in Fig. 3b; (d) EDX results for three phase.

Fig. 4 Effect of Cu on Electrochemical Impedance Spectroscopy (EIS) of CADI in solutions with pH = 4

Fig. 5 Influence of Cu content on the corrosive wear: (a) pH = 4, (b) pH = 10, (c) Cumulative wear loss versus Cu content for both pH values (10 h)

Fig. 6 Influence of Cu content on the wear loss of CWWL tests

Fig. 7 Potential map scanning by AFM (a) 0 wt.% Cu; (b) 1.5 wt.% Cu; Around carbides (1.5 wt.% Cu);

Fig. 8 SEM image and surface scanning results of CADI after the corrosion of acid solution: (a) SEM image; (b) SEM image at high magnification (c) C; (d) Cu; (e) Fe; (f) O

Fig. 9 SEM image and surface scanning results of CADI after the corrosion of alkaline solution: (a) SEM image; (b) SEM image of corrosion products; (c) C; (d) O; (e) Mg; (f) Fe

Fig.10 XPS analyzing results of Cu-free CADI after soaked by the solution of pH =

10: (a) Fe 2p; (b) O 1s, (c) Cr 2p

Fig.11 XPS analyzing results of CADI with 1.5 wt% Cu after soaked by the solution of pH = 10: (a) Fe 2p; (b) O 1s, (c) Cr 2p; (d) Cu 2p

Fig.12 SEM images and 3D laser morphologies of CADI corrosive worn surfaces: (a) SEM images of Cu-free CADI, pH = 4; (b) SEM images of CADI with 1.5 wt.% Cu, pH = 4; (c) SEM images of Cu-free CADI, pH = 10; (d) SEM images of CADI with 1 wt.% Cu, pH = 10; (e) 3D laser morphologies of Cu-free CADI, pH = 4; (f) 3D laser morphologies of CADI with 1 wt.% Cu, pH = 4; (g) 3D laser morphologies of Cu-free CADI, pH = 10; (h) 3D laser morphologies of CADI with 1 wt.% Cu, pH = 10; (i) CADI corrosive wear depth.

Fig.13 SEM images and 3D laser morphologies of CADI surfaces after CWWL tests: (a) SEM images of Cu-free CADI, pH = 4; (b) SEM images of CADI with 1 wt.% Cu, pH = 4; (c) SEM images of Cu-free CADI, pH = 10; (d) SEM images of CADI with 1 wt.% Cu, pH = 10; (e) 3D laser morphologies of Cu-free CADI, pH = 4; (f) 3D laser morphologies of CADI with 1 wt.% Cu, pH = 4; (g) 3D laser morphologies of Cu-free CADI, pH = 10; (h) 3D laser morphologies of CADI with 1 wt.% Cu, pH = 10; (i) CADI wear depth after CWWL tests:

Figure 1

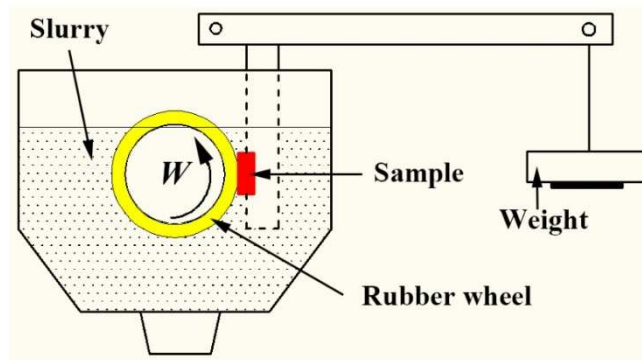


Fig 1 Schematic diagram of corrosive wear with load test (CWLL test)

Figure 2

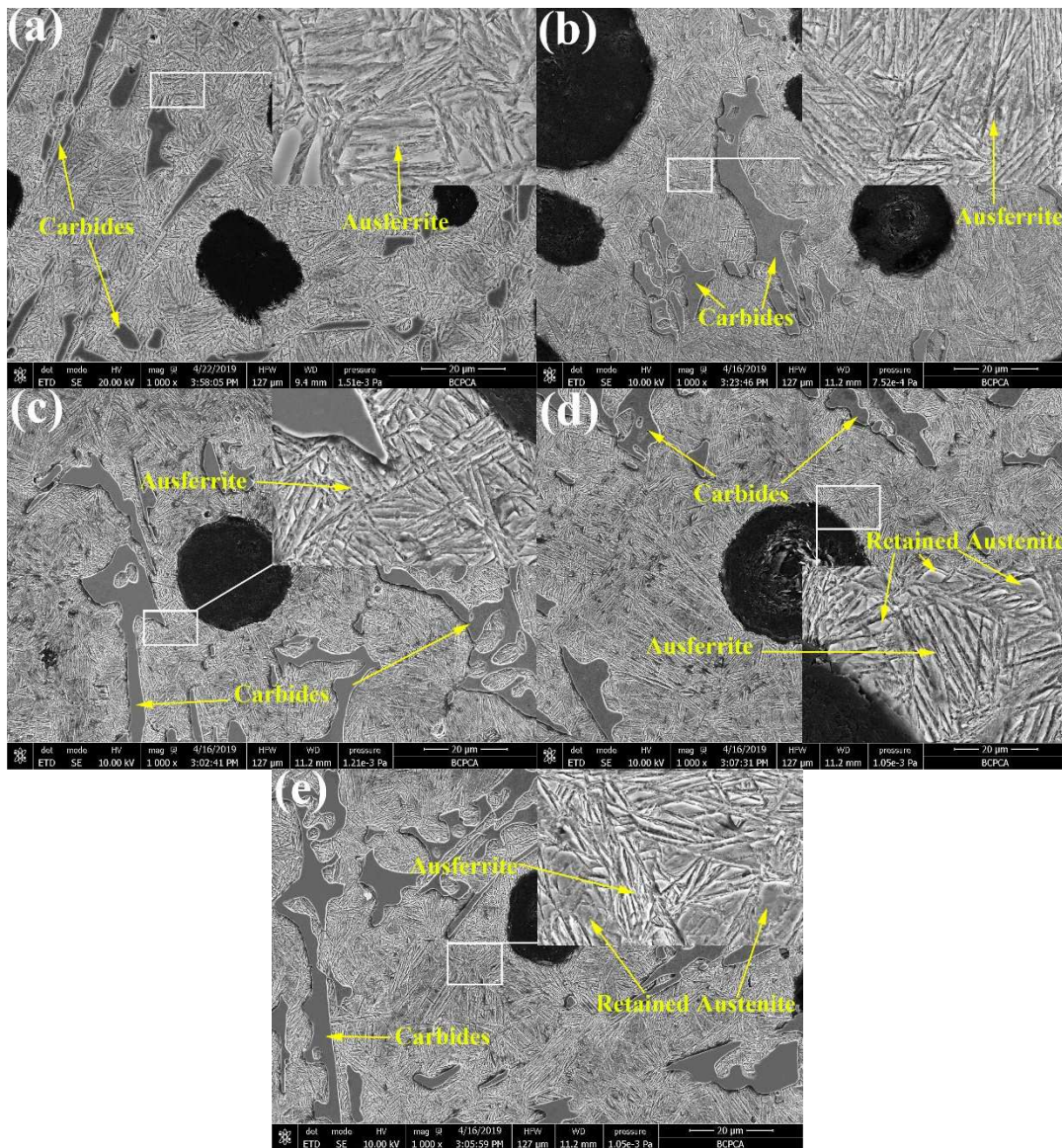


Fig. 2 SEM images of CADI for different Cu content: (a) 0 wt.% Cu; (b) 0.5 wt.%

Cu; (c) 1 wt.% Cu; (d) 1.5 wt.% Cu; (e) 2 wt.% Cu;

Figure 3

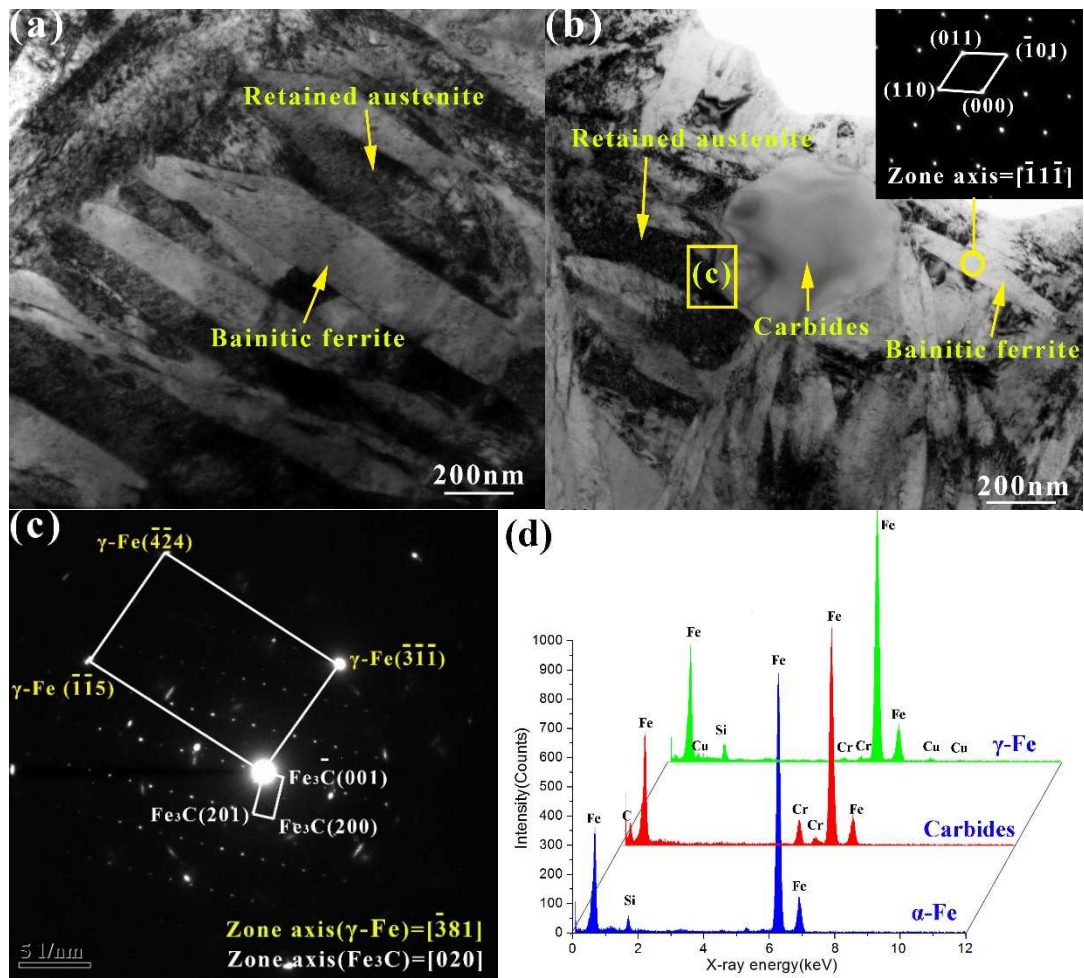


Fig. 3 TEM images of Cu-bearing CADI: (a) Bright-field TEM micrographs of Cu-free CADI; (b) Bright-field TEM micrographs of CADI with 2.0 wt.% Cu; (c) Selected area diffraction patterns (SADPs) of area C in Fig. 3b; (d) EDX results for three phase.

Figure 4

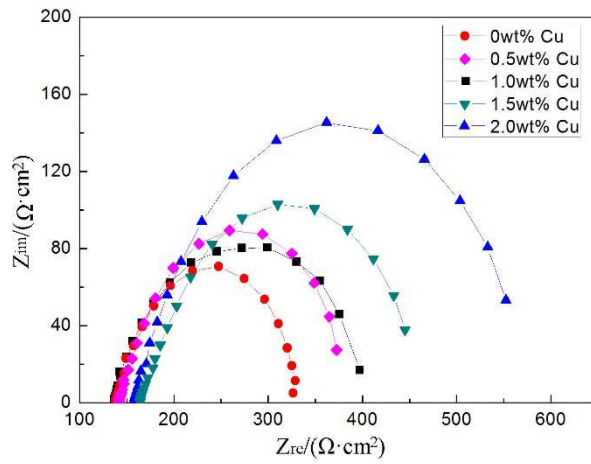


Fig. 4 Effect of Cu on Electrochemical Impedance Spectroscopy (EIS) of CADI in solutions with pH = 4

Figure 5

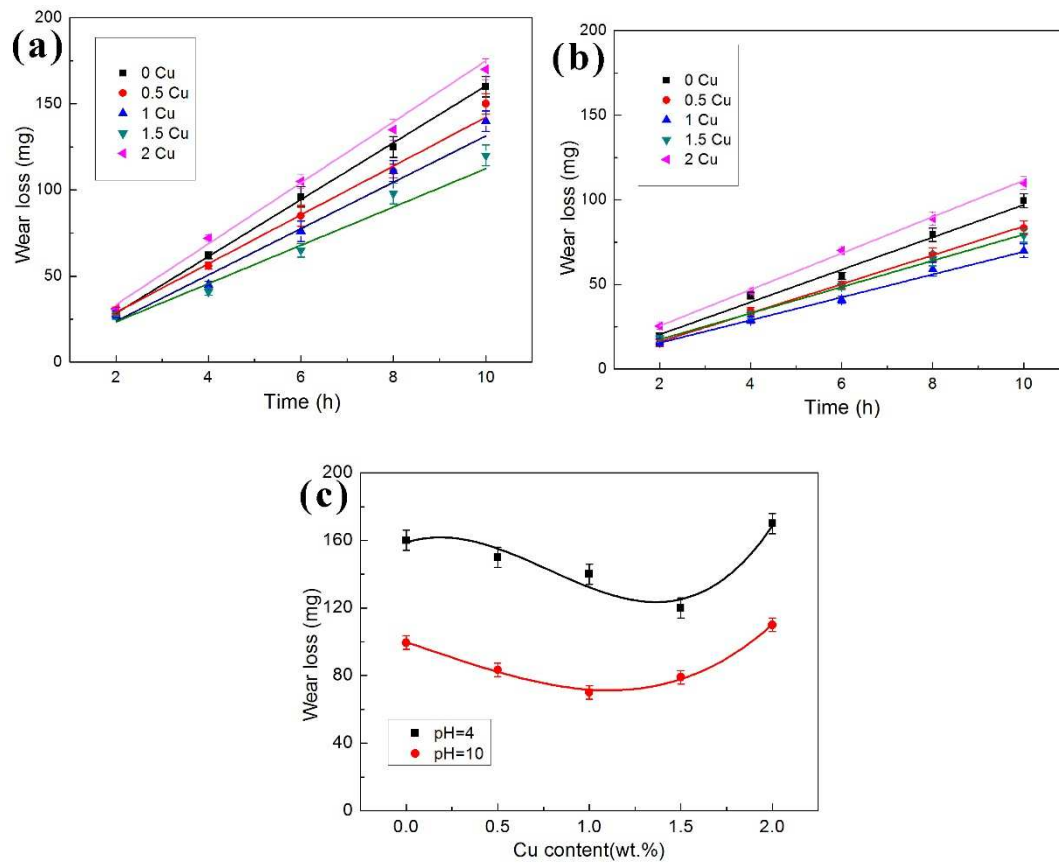


Fig. 5 Influence of Cu content on the corrosive wear: (a) pH = 4, (b) pH = 10, (c) Cumulative wear loss versus Cu content for both pH values (10 h).

Figure 6

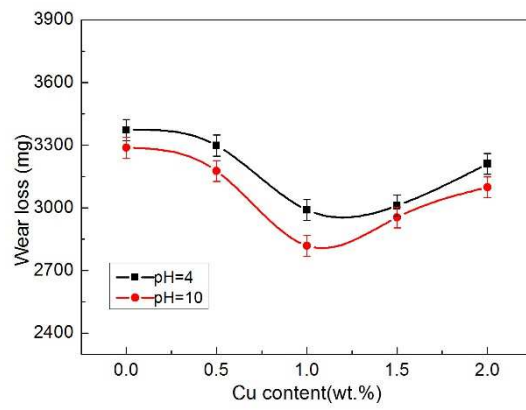


Fig. 6 Influence of Cu content on the wear loss of CWWL tests

Figure 7

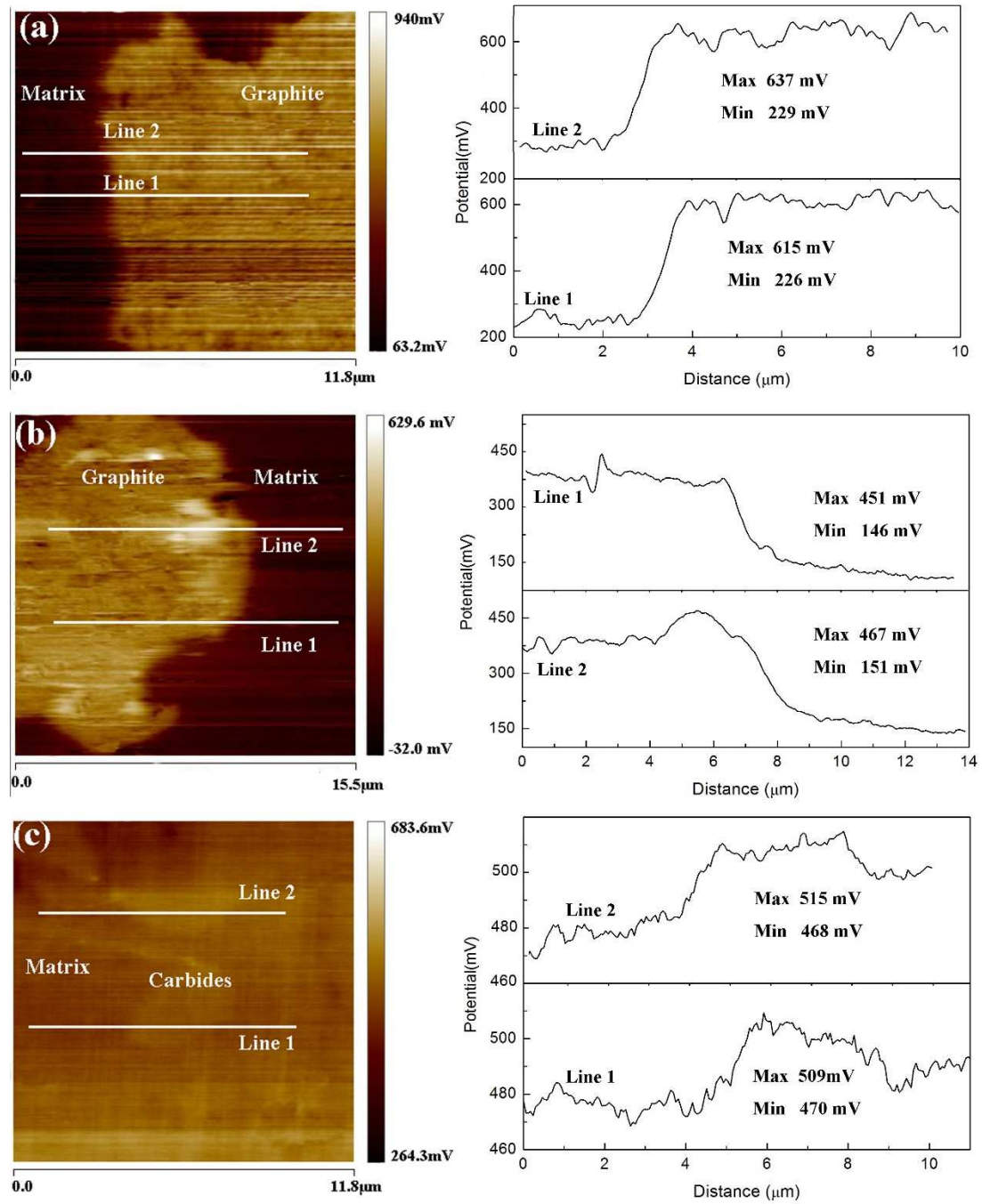


Fig. 7 Potential map scanning by AFM (a) 0 wt.% Cu; (b) 1.5 wt.% Cu; Around carbides (1.5 wt.% Cu);

Figure 8

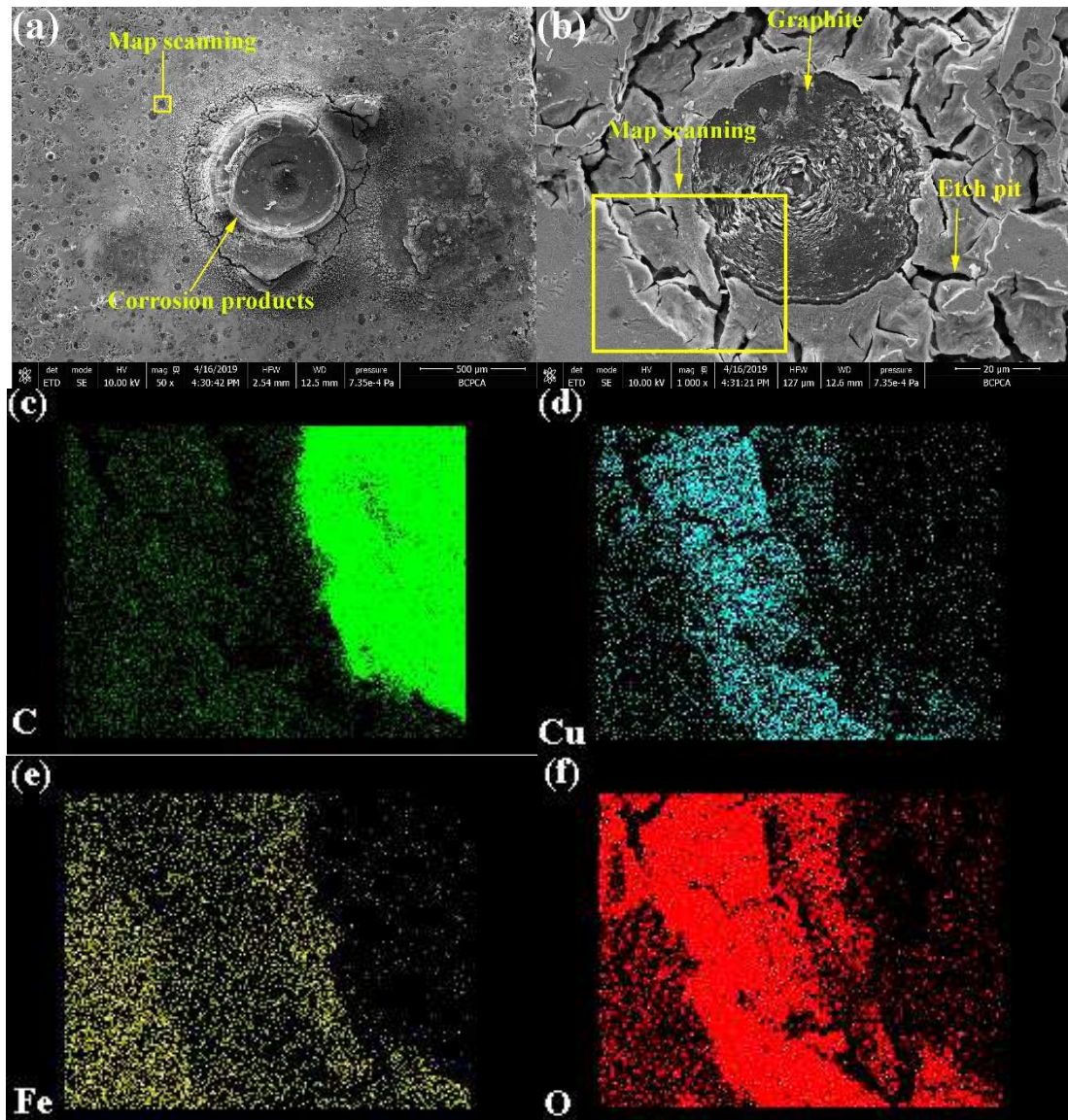


Fig. 8 SEM image and surface scanning results of CADI after the corrosion of acid solution: (a) SEM image; (b) SEM image at high magnification (c) C; (d) Cu; (e) Fe; (f) O

Figure 9

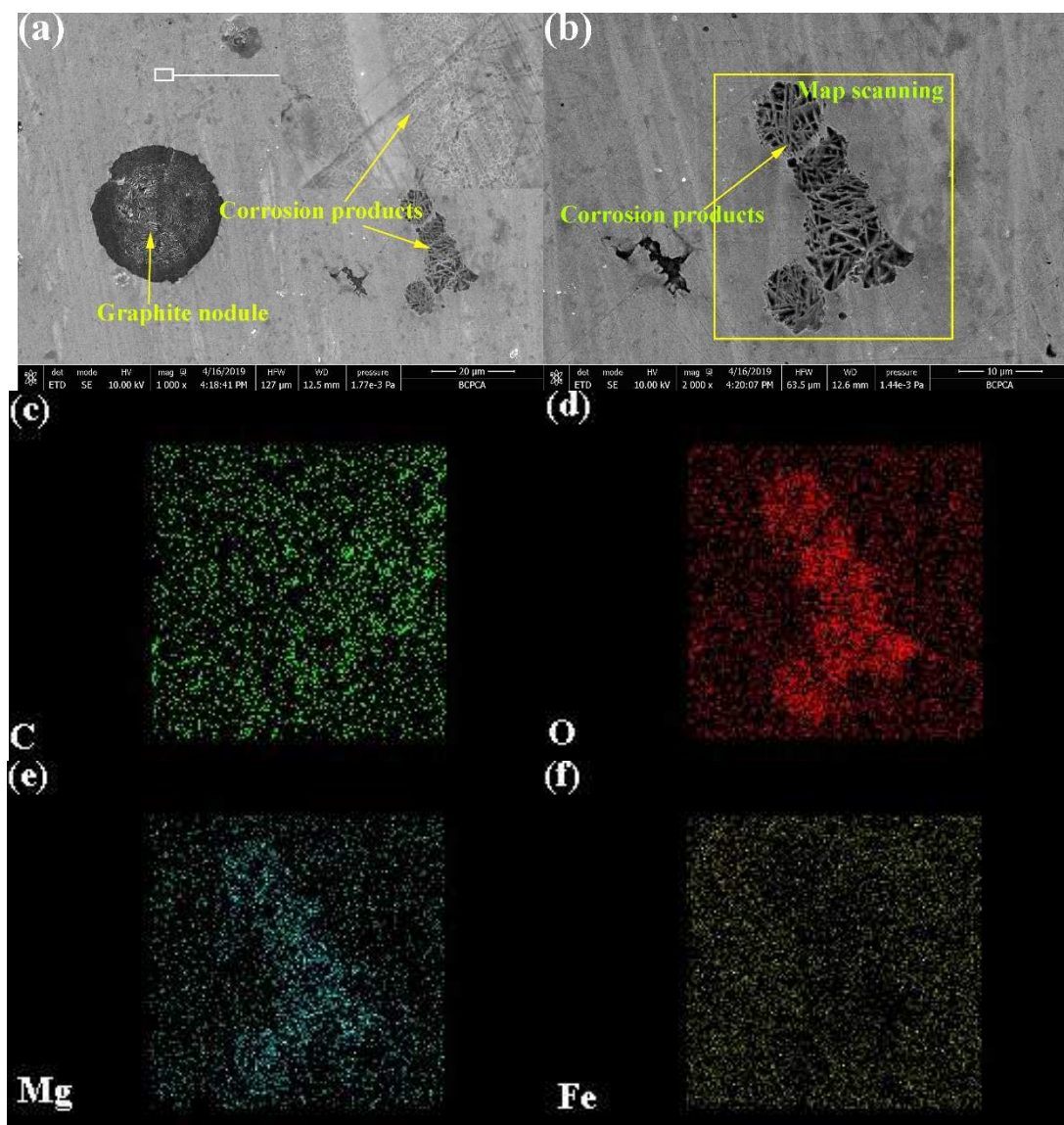


Fig. 9 SEM image and surface scanning results of CADI after the corrosion of alkaline solution: (a) SEM image; (b) SEM image of corrosion products; (c); C; (d) O; (e) Mg; (f) Fe

Figure 10

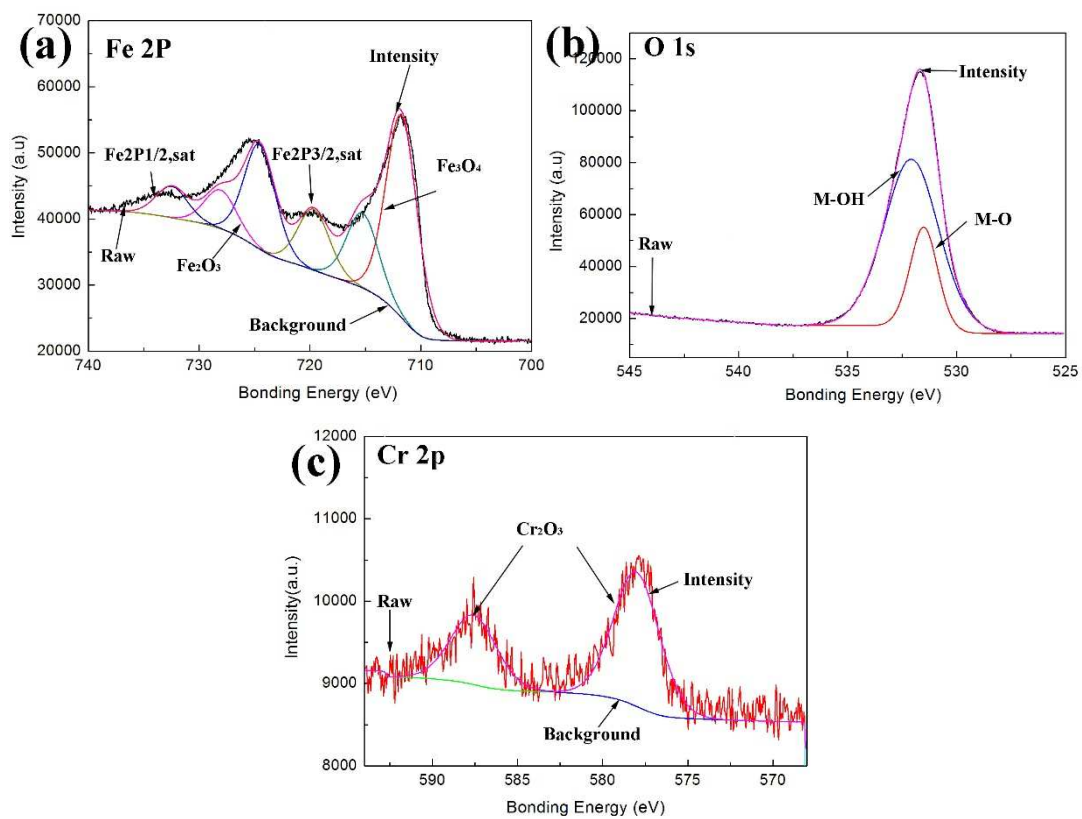


Fig.10 XPS analyzing results of Cu-free CADI after soaked by the solution of pH =

10: (a) Fe 2p; (b) O 1s, (c) Cr 2p

Figure 11

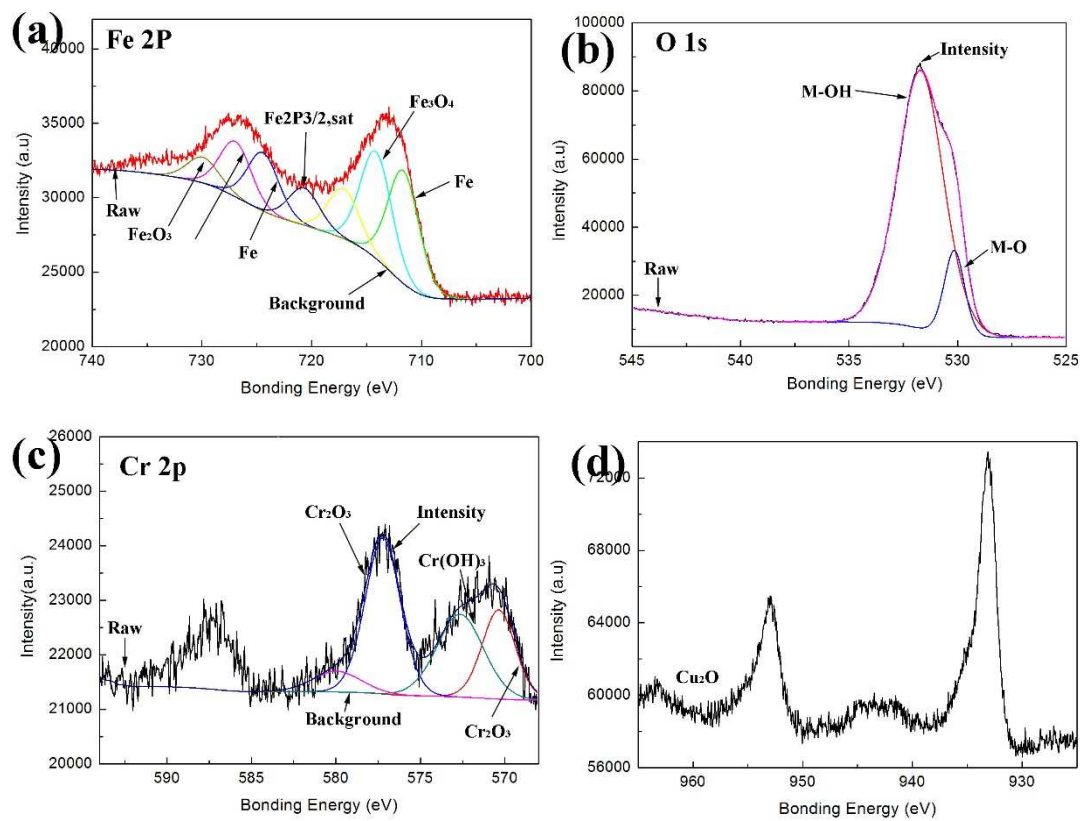
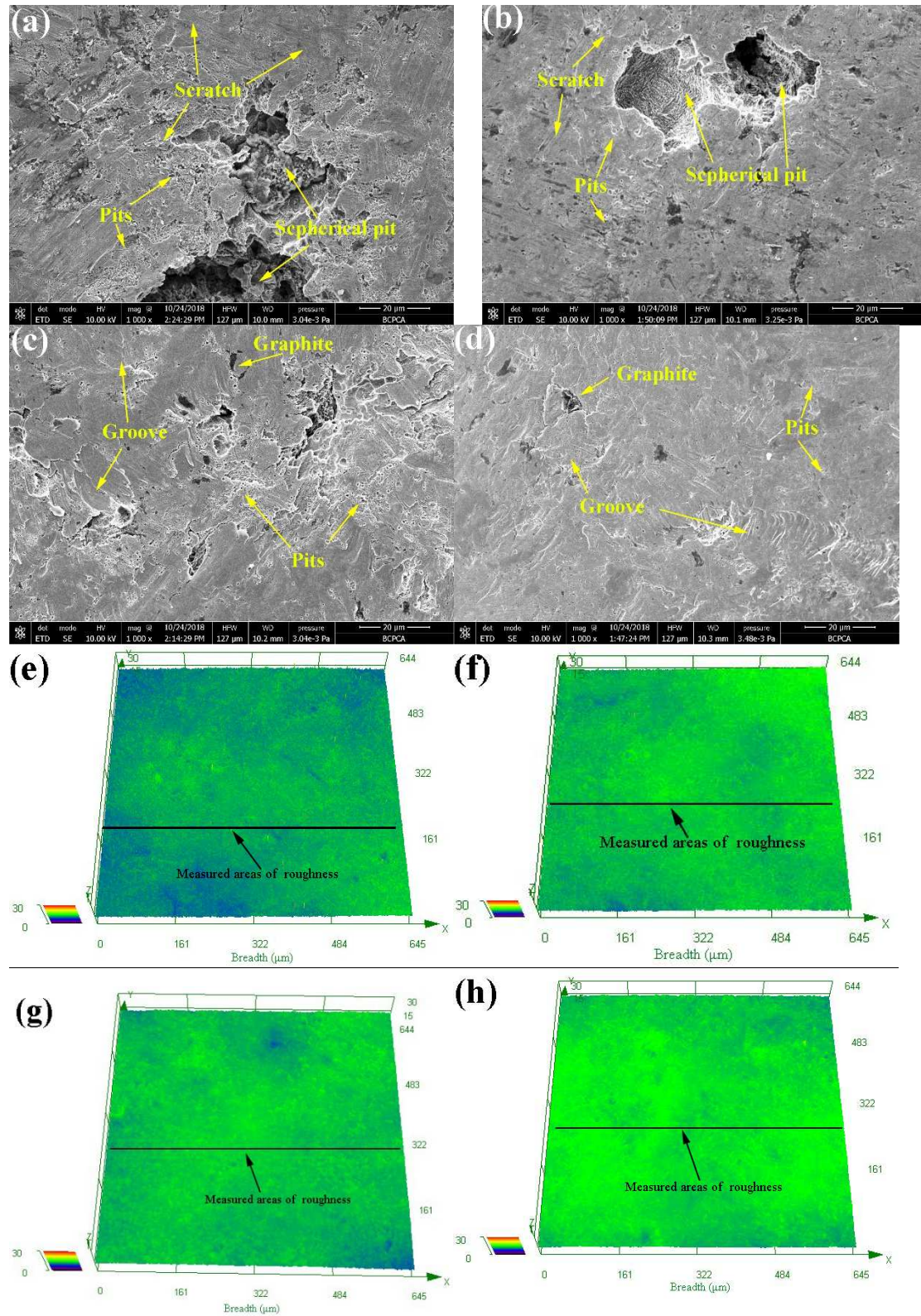


Fig.11 XPS analyzing results of CADI with 1.5 wt% Cu after soaked by the solution of pH = 10: (a) Fe 2p; (b) O 1s, (c) Cr 2p; (d) Cu 2p

Figure 11



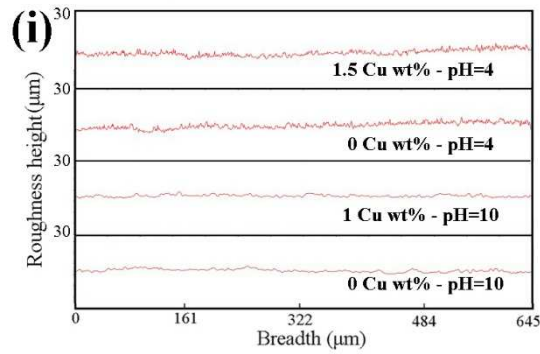
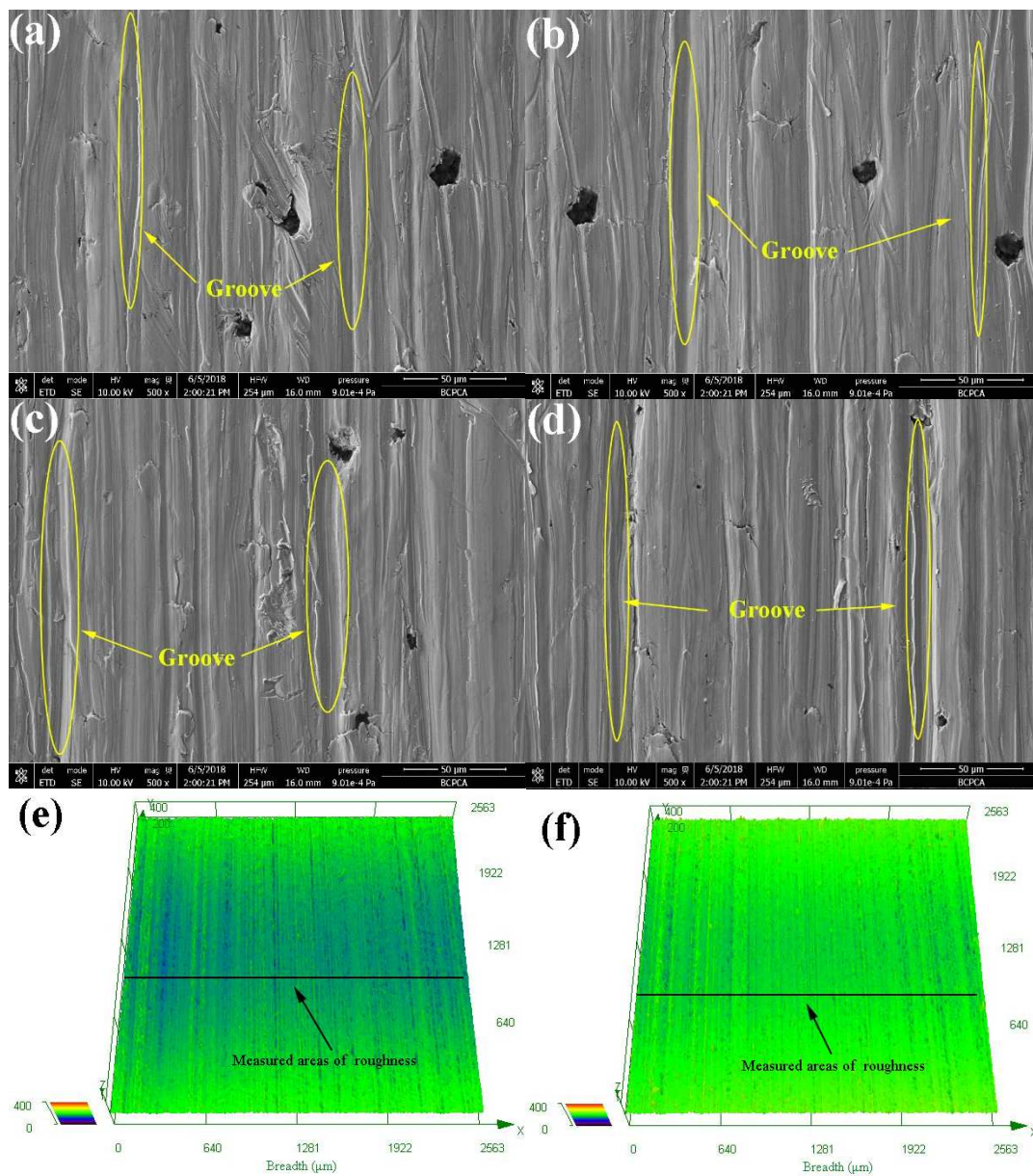


Fig.12 SEM images and 3D laser morphologies of CADI corrosive worn surfaces: (a) SEM images of Cu-free CADI, pH = 4; (b) SEM images of CADI with 1.5 wt.% Cu , pH = 4; (c) SEM images of Cu-free CADI, pH = 10; (d) SEM images of CADI with 1 wt.% Cu, pH = 10; (e) 3D laser morphologies of Cu-free CADI, pH = 4; (f) 3D laser morphologies of CADI with 1 wt.% Cu, pH = 4; (g) 3D laser morphologies of Cu-free CADI, pH = 10; (h) 3D laser morphologies of CADI with 1 wt.% Cu, pH = 10; (i) CADI corrosive wear depth.

Figure 13



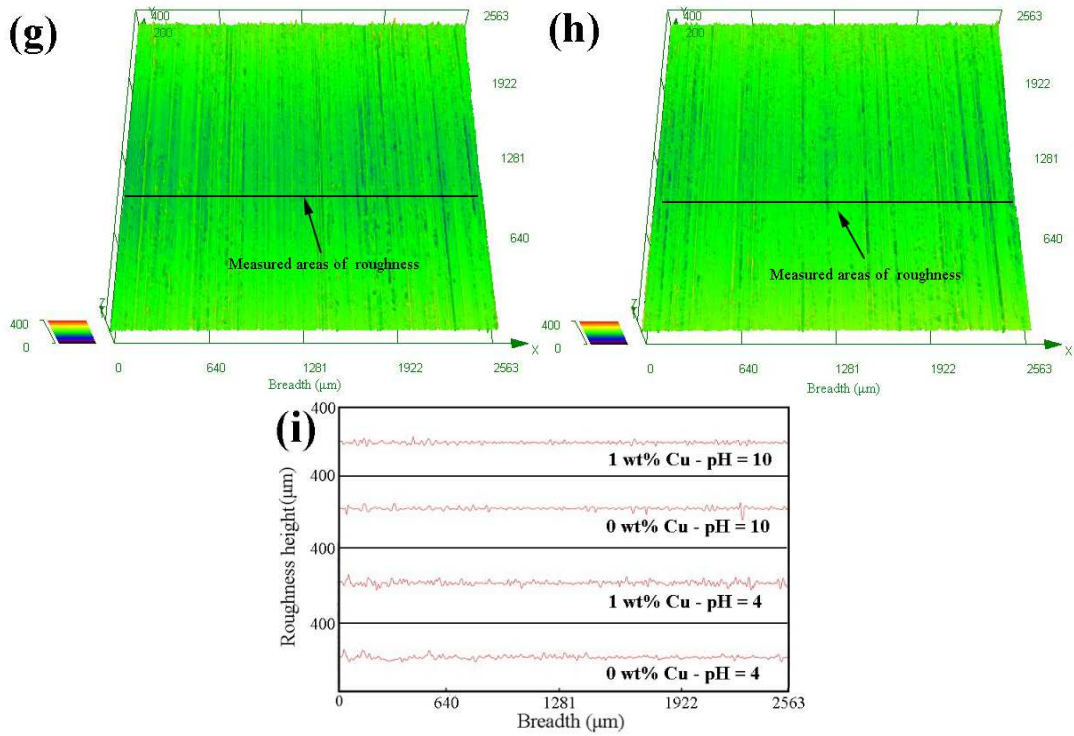


Fig.13 SEM images and 3D laser morphologies of CADI surfaces after CWWL tests:
 (a) SEM images of Cu-free CADI, pH = 4; (b) SEM images of CADI with 1 wt.% Cu, pH = 4; (c) SEM images of Cu-free CADI, pH = 10; (d) SEM images of CADI with 1 wt.% Cu, pH = 10; (e) 3D laser morphologies of Cu-free CADI, pH = 4; (f) 3D laser morphologies of CADI with 1 wt.% Cu, pH = 4; (g) 3D laser morphologies of Cu-free CADI, pH = 10; (h) 3D laser morphologies of CADI with 1 wt.% Cu, pH = 10; (i) CADI wear depth after CWWL tests: